A Theoretical Study of the Kinetics of the Benzylperoxy Radical Isomerization

Sébastien Canneaux,* Florent Louis,* Marc Ribaucour, Rodolphe Minetti, Abderrahman El Bakali, and Jean-François Pauwels

PhysicoChimie des Processus de Combustion et de l'Atmosphère (PC2A) UMR CNRS 8522, FR CNRS 2416 Centre d'Etudes et de Recherche Lasers et Applications (CERLA), and Université des Sciences et Technologies de Lille, 59655 Villeneuve d'Ascq Cedex, France

Received: November 27, 2007; Revised Manuscript Received: March 27, 2008

The rate constant of the benzylperoxy isomerization reaction has been computed using 54 different levels of theory and has been compared to the experimental value reported at 773 K. The aim of this methodology work is to demonstrate that standard theoretical methods are not adequate to obtain quantitative rate constants for the reaction under study. The use of the elaborated CASPT2 method is essential to estimate a quantitative rate constant. Geometry optimizations and vibrational frequency calculations are performed using three different methods (B3LYP, MPW1K, and MP2) and six different basis sets (6-31G(d,p), 6-31+G(d,p), 6-31++G(d,p), 6-311G(d,p), 6-311+G(d,p), and cc-pVDZ). Single-point energy calculations are performed with the highly correlated ab initio coupled cluster method in the space of single, double, and triple (pertubatively) electron excitations CCSD(T) using the 6-31G(d,p) basis set, and with the CASPT2 level of theory with the ANO-L-VDZP basis set. Canonical transition-state theory with a simple Wigner tunneling correction is used to predict the high-pressure limit rate constants as a function of temperature. We recommend the use of the CASPT2/ANO-L-VDZP//B3LYP/cc-pVDZ level of theory to compute the temperature dependence of the rate constant of the four-center isomerization of the benzylperoxy radical. It is given by the following relation: $k(600-2000\ \text{K})\ (\text{in}\ \text{s}^{-1}) = (1.29 \times 10^{10})\ T^{0.79} \exp[(-133.1\ \text{in kJ mol}^{-1})/RT]$. These parameters can be used in the thermokinetic models involving aromatic compounds at high pressure. This computational procedure can be extended to predict rate constants for other similar reactions where no available experimental data exist.

I. Introduction

Aromatic compounds are currently used in everyday life. For example, they are used as solvents and are components of automotive and aeronautical fuels. Their percentage in mass in a European gasoline, a Californian reformulated gasoline, a diesel fuel, and a jet fuel are 35, 31, 30, and 15%, respectively.[1] The European directive 2003/17/CE[2] fixed the maximum amount of benzene to 1% in volume in gasoline and for other aromatic compounds to 35%; in diesel fuel the amount of polyaromatic compounds must not exceed 11% in mass. The presence of aromatic compounds in gasoline is desirable because they have high octane numbers. It must be noted that combustion systems using fossil fuels can emit under certain conditions aromatic compounds, even if the fuel composition does not contain any. Aromatic compounds are at the origin of polycyclic aromatic hydrocarbon (PAH) and soot particle formation as reported in many studies.[3–15] Toxicological studies show that some of these PAHs (especially benzo(*a*)pyrene, fluoranthene, and cyclopenta-[*c,d*]pyrene) have mutagenic and carcinogenic properties.[16–18]

Useful properties of aromatic compounds and their negative impact on environment and health have motivated many studies on their oxidation process. These studies have been mainly devoted to the simplest monoaromatic compounds, which are benzene and toluene. We have recently pointed out the major studies on this topic in two articles.[19,20] The main objective of these studies was to identify the formation and/or destruction pathways of aromatic compounds by means of detailed thermokinetic model validation. Detailed kinetic mechanisms of these models contain hundreds of elementary reactions and about 100 chemical species. The assignation of thermochemical data to species and kinetic rate constants to reactions is a complicated task because of the lack of information in the literature. This task is rendered more difficult because thermokinetic data must be known in large ranges of pressure and temperature to allow the use of thermokinetic models in conditions encountered in practical combustion systems. For example, temperature varies from 500 to 2500 K and pressure from 1 to about 60 bar in the combustion chamber of a spark ignition engine. Pressure has an influence on the rate constant of reactions exhibiting a falloff behavior and on rate of reactions requiring a third body. Temperature influences almost all reactions and modifies considerably the oxidation pathways. It is now well identified that a low-, an intermediate-, and a high-temperature oxidation mechanism exist.[21,22] In automotive and aeronautical engines, the three mechanisms are implied because of the large range of temperatures encountered.

Many studies have been performed on the development of high-temperature oxidation thermokinetic models in our laboratory.[19,20,23–26] Some of these models relate to formation and/or thermal depletion of benzene[20] and toluene[19] in premixed flames. Low-temperature oxidation thermokinetic models have been also elaborated in our laboratory: they concern *n*-butane,[27] *n*-pentane,[28] pent-1-ene,[28] *n*-butylbenzene,[29] and cyclohexene.[30] We have also built an oxidation thermokinetic model for methane/benzene and *n*-heptane/benzene mixtures.[20] This model has been tested against experimental data obtained at low and

* To whom correspondence should be addressed. Telephone: (33)3-20436977. E-mail: sebastien.canneaux@univ-lille1.fr; florent.louis@univ-lille1.fr.

10.1021/jp711231c CCC: $40.75
Published on Web 06/11/2008

high temperatures and at sub- and upper-atmospheric pressures. If benzene does not react at low temperature as shown in ref,[20] aromatic compounds with an alkyl side chain (such as toluene, *o*-xylene, and ethylbenzene) exhibit a low-temperature reactivity.[31–33] However, with the exception of *n*-butylbenzene,[29] only high-temperature oxidation thermokinetic models have been published for these aromatic compounds.[34–51] It is not surprising because of the considerable lack of experimental data for low-temperature reactions of aromatic compounds. Determination of thermochemical data and kinetic parameters by means of quantum chemistry tools is a valuable solution to fill in the absence of experimental data. This article is the first one of a series devoted to the generation of thermokinetic data for alkyl side-chain aromatic compounds (namely, toluene and xylene isomers) by using quantum chemistry methods, statistical thermodynamics, and canonical transition-state theory. These new thermokinetic data will be included later in low-temperature oxidation thermokinetic models developed in our laboratory.

At low temperature, addition of molecular oxygen to aryl radicals ($C_6H_5-\dot{R}$) occurs in the oxidation process of alkylbenzenes (C_6H_5-RH):

$$C_6H_5-\dot{R}+O_2=C_6H_5-R\dot{O}_2 \qquad (R1)$$

This reaction is an equilibrium that is very sensitive to the temperature. It shifts toward the products $C_6H_5-\dot{R}+O_2$ when temperature overcomes the "ceiling temperature", this later depending on the structure of $C_6H_5-\dot{R}$ and $C_6H_5-R\dot{O}_2$ radicals and O_2 partial pressure.[52] Reaction R1 is followed by an internal H-atom transfer producing an aryl hydroperoxide radical $C_6H_5-\dot{Q}O_2H$:

$$C_6H_5-R\dot{O}_2=C_6H_5-\dot{Q}O_2H \qquad (R2)$$

The internal transfer is easier when the transferred hydrogen atom is benzylic.[29] In the case of toluene, the only possible transfer is a 1,3sb transfer involving one of the two secondary benzylic hydrogen atoms of benzylperoxy radical:

$$C_6H_5-CH_2\dot{O}_2=C_6H_5-\dot{C}HO_2H \qquad (R3)$$

In the notation 1,3sb, Number 1 indicates the position of the radical oxygen; Number 3 indicates the relative position of the carbon atom bonded to the transferred hydrogen atom. The letter s stands for secondary and the letter b for benzylic. After formation by reaction R3, the benzyl hydroperoxide radical decomposes to yield benzaldehyde and $\dot{O}H$ radical by the following reaction:

$$C_6H_5-\dot{C}HO_2H=C_6H_5-CHO+\dot{O}H \qquad (R4)$$

Benzaldehyde has been identified as a major oxidation product of pure toluene or alkane/toluene mixtures in studies at temperature below 800 K: in a static reactor between 723 and 788 K,[31] in a jet-stirred reactor between 580 and 620 K,[32] and in a rapid compression machine at 750 K.[53] The reaction sequence R1−R3−R4 is often suggested to explain the benzaldehyde formation in the low-temperature oxidation mechanism of toluene.

In the reaction sequence R1−R3−R4, reaction R3 is certainly the rate-limiting step as it involves a strained four-center cyclic transition state. Thus, a reliable value for the rate constant of this reaction is needed. In the literature, only one experimental determination of this rate constant is available.[54] It is a measurement based on an indirect method using addition of toluene to mixtures of H_2 and O_2. The reported rate constant value is 2.8×10^3 s^{-1} at 773 K under 0.67 bar total pressure. This experimental value will be used to validate our theoretical methodology for the estimation of the rate constant.

A few theoretical studies have been carried out on the reactions of four-center isomerization of the alkylperoxy[55–59] and arylperoxy[60] radicals. Chan et al.[55] performed BHandHLYP/6-311G(d,p) calculations estimating the activation energies and pre-exponential factors for a series of intramolecular hydrogen-atom abstraction reactions in aliphatic peroxyl radicals containing up to five carbons. In particular, the calculated activation energy by Chan et al.[55] was about 209 kJ mol^{-1} for the four-center isomerization reaction of the pentylperoxy radical. Sheng et al.[56] studied the detailed kinetics and thermochemistry for the reaction between the C_2H_5 ethyl radical and molecular oxygen. The isomerization transition state (TS) of the ethylperoxy adduct ($CH_3-CH_2\dot{O}_2$) leading to the formation of acetaldehyde (CH_3CHO) and OH radical was characterized at the B3LYP/6-31G(d,p) level of theory. The energy barrier was estimated at 0 K to 174.7 kJ mol^{-1} at the CBS-Q//B3LYP/6-31G(d,p) level of theory. Sun and Bozzelli[57] worked on the reactions of neopentyl and neopentyl hydroperoxide radicals with molecular oxygen. Part of this study concerned the four-center isomerization of the neopentylperoxy radical ($C_4H_9-CH_2\dot{O}_2$) for which the CBS-Q reaction barrier was 174.0 kJ mol^{-1}. Lee and Bozzelli[58] studied the reaction of the allyl radical with molecular oxygen. The thermochemical and kinetic parameters were obtained using the CBS-Q composite method. The energy barrier of the four-center isomerization was estimated to 157.9 kJ mol^{-1}. Zhu et al.[59] performed theoretical calculations at the CBS-QB3 on the kinetics of the intramolecular hydrogen shift reactions of the butylperoxy ($C_3H_7-CH_2\dot{O}_2$) and pentylperoxy ($C_4H_9-CH_2\dot{O}_2$) radicals. Both energy barriers of the four-center isomerizations were estimated at 0 K to 170.7 kJ mol^{-1}. It is worth noticing that, in all these mentioned studies,[56–59] no structure for the alkyl hydroperoxide radicals was characterized. Clothier et al.[60] worked on the simulation of diesel fuel ignition by benzyl radicals and showed, by using ab initio molecular orbital calculations, that there is a plausible mechanism by which benzylperoxy radical thermal decomposition could lead to the production of OH radicals. The calculations were done at the low level of theory ROMP2/3-21G//ROHF/3-21G. The pre-exponential factor and the activation energy for the benzylperoxy radical isomerization were estimated to be 10^{13} s^{-1} and 121 kJ mol^{-1}, respectively.

A very recent theoretical study was performed by Murakami et al.[61] to determine the kinetics, the mechanism, and the product branching ratios of the benzyl + O_2 reaction at the CBS-QB3 level of theory. The authors found that the reaction proceeded with an exothermic barrierless addition of molecular oxygen to the benzyl radical to form the benzylperoxy radical. The benzylperoxy radical can be dissociated (i) backward with a 93.3 kJ mol^{-1} energy barrier (called channel E in their article), (ii) into the $C_6H_4CH_2OOH$ radical with a 135.6 kJ mol^{-1} energy barrier (channel C), (iii) into the cyclic O_2 adduct with a 128.0 kJ mol^{-1} energy barrier (channel D), and (iv) leading to the formation of benzaldehyde and OH radical with a 161.9 kJ mol^{-1} energy barrier (channel B), which is higher than the one predicted by Clothier et al.[60] In the reaction system of the O_2 addition to the allyl radical, Lee and Bozzelli[58] reported energy barriers for the same channels that were very close to the ones obtained by Murakami et al.[61] The temperature dependence of the high-pressure limit rate constant for these reaction

channels was computed by Murakami et al.[61] to be between 300 and 1500 K.

In this work, highly correlated quantum chemical calculations were performed to directly compute the barrier for reaction R3 without any energy adjustments. The energetics of the reactant and the TS was used together with transition state theory (TST) calculations to compute the rate constants in the temperature range 600−2000 K. To our knowledge, this is the first time that the temperature dependence of the rate constant for the benzylperoxy radical isomerization has been computed at a highly correlated level of theory.

This article is organized as follows. Computational methods are reported in section II, and the results are presented and discussed in section III.

II. Computational Methods

Ab initio and DFT calculations were performed using the Gaussian03[62] and MOLCAS 6.0[63] software packages. Reactant and TS structures were fully optimized at HF-DFT (B3LYP),[64,65] MPW1K,[66] and MP2[67] levels of theory using the following Pople-style 6-31G(d,p), 6-31+G(d,p), 6-31++G(d,p), 6-311G(d,p), and 6-311+G(d,p) basis sets[68] and Dunning's correlation consistent double-ζ plus polarization cc-pVDZ[69] basis set. Product geometries were fully optimized at MPW1K and MP2 levels of theory with the same six basis sets. All TSs have been characterized by one imaginary frequency (first-order saddle points) on the potential energy surface. Special care was taken to determine minimum energy pathways, performing intrinsic reaction coordinate (IRC) analyses[70] using all levels of theory, to confirm that a specific TS connects the different local minima. Vibrational frequencies were determined within the harmonic approximation, at the same level of theory as for geometries. For the reactant and TS structures, single-point energy calculations were carried out at different high levels of theory using in each case the optimized B3LYP, MPW1K, and MP2 geometrical parameters. Electron correlation was calculated with second Møller−Plesset perturbation theory with full annihilation of spin contamination[71] as implemented in the GAUSSIAN package (noted in our results as PMP2). Thus, electronic energies were obtained: (i) employing the single and double coupled cluster theory with inclusion of a perturbative estimation for triple excitation[72–75] (CCSD(T)) with the 6-31G(d,p) basis set (the frozen-core approximation has been applied in CCSD(T) calculations, which implies that the inner shells are excluded at estimating the correlation energy), and (ii) CASPT2 [76–79] level of theory with the ANO-L-VDZP[80] basis set. In this work, it is necessary to obtain energy differences between the TS and the reactant at a high level of theory such as, for example, CCSD(T) or CASPT2, particularly to carry out rate constant calculations through TST at a later stage. The cost of optimizing geometries at these levels can be very prohibitive. In these conditions, it is helpful to perform calculations at a higher level of theory using the geometries optimized at a lower level. The CASPT2 method was carried out to incorporate both dynamic and nondynamic correlation effects on the relative energy ordering of the calculated stationary points. The CASPT2 approach is based on a second-order perturbation treatment where the CASSCF wavefunction is taken as the reference function. Thus, the parameters of the CASPT2/CASSCF calculations are those of the CASSCF step. In this study, single-point CASPT2/CAS(3,3) calculations were obtained using again the ANO-L-VDZP basis set on the optimized geometries and excluding inner shells and corresponding virtual counterpart from the perturbation calculation. For the abstraction mechanism, the active space (3,3) that best describes the C−H bond breaking and O−H bond forming includes the σ_{C-H} bonding molecular orbital (MO) with the associated σ^*_{C-H} antibonding MO and the single electron MO.

Canonical TST[81] was used to predict the temperature dependence of the rate constants. Accordingly, the high-pressure limit rate constants, $k(T)$, were computed using the following expression:

$$k(T) = \Gamma(T) \times \frac{k_B T}{h} \times \frac{Q_{TS}(T)}{Q_{\text{benzylperoxy radical}}(T)} \times \exp\left(-\frac{E_0}{k_B T}\right) \quad \text{(II-1)}$$

where $\Gamma(T)$ indicates the transmission coefficient used for the tunneling correction at temperature T, and the terms $Q_{TS}(T)$ and $Q_{\text{benzylperoxy radical}}(T)$ are the total partition functions for the TS and the benzylperoxy radical at temperature T. In eq II-1, the vibrationally adiabatic barrier height, E_0, is computed as the energy difference between the TS and the reactant, including zero-point energy corrections. k_B is Boltzmann's constant, and h is Planck's constant.

The calculation of the reaction rate constants using the TST formulation given by eq II-1 requires the proper computation of the partition functions of the reactant and the TSs. The total partition function $Q^X(T)$ of a species X can be cast in terms of the translational $Q^X_T(T)$, electronic $Q^X_e(T)$, rotational $Q^X_R(T)$, and vibrational $Q^X_V(T)$ partition functions:

$$Q^X(T) = Q^X_T(T) Q^X_e(T) Q^X_R(T) Q^X_V(T) \quad \text{(II-2)}$$

In this work, we adopt the simple and computationally inexpensive Wigner method[82] in the calculation of all tunneling corrections for the reactions reported here:

$$\Gamma(T) = 1 + \frac{1}{24}\left(\frac{h\nu^{\ddagger}}{k_B T}\right)^2 \quad \text{(II-3)}$$

where $\nu^{\ddagger}$ is the imaginary frequency at the saddle point. This choice seems to be appropriate to the tunneling corrections applied to rate constants at typical incineration/combustion temperatures (600−2000 K) for which the values of transmission coefficients $\Gamma(T)$ are small to moderate (≤ 2).[59,83] More sophisticated and computationally demanding algorithms such as the ones developed by Truhlar et al.[84] and Miller et al.[85] should be used if the transmission coefficients are much higher than the ones computed in this study. The rate constant calculations were performed over the temperature range of interest using the KISTHEP software suite.[86]

III. Results and Discussion

III.1. Geometric Parameters and Vibrational Frequencies.

Geometric Parameters. Figure 1 shows the structures and atom numbering of the reactant (benzylperoxy radical), the isomerization TS, and the product (benzyl hydroperoxide radical). Table 1 gathers the selected bond lengths calculated at the different levels of theory. More detailed information regarding optimized geometric parameters for these species is presented in Tables 1S−8S of the Supporting Information.

Benzylperoxy Radical. At all levels of theory, the global minimum for the benzylperoxy radical is found to be in a conformation in which the dihedral angles $C_3C_2C_1O_2$ and $C_2C_1O_2O_1$ are equal to about −90° and 180°, respectively. The

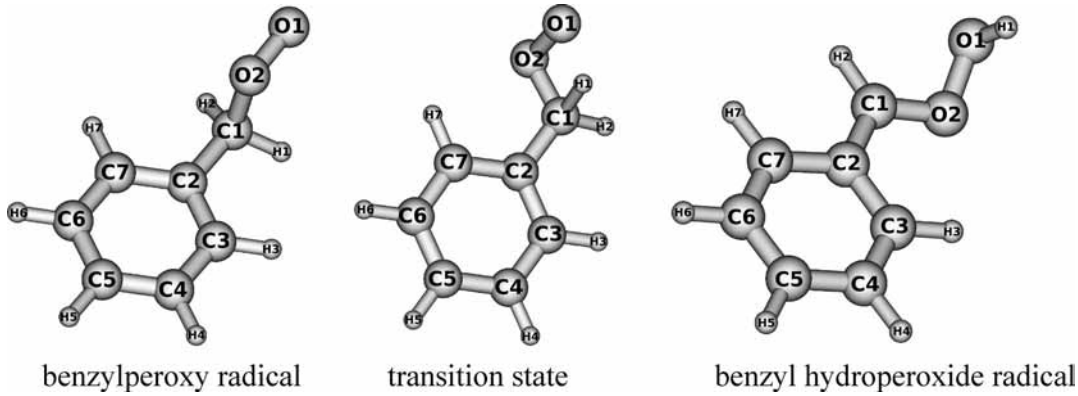

Figure 1. Structure and atom numbering of the different species involved in the reaction.

same results were obtained by Garcia et al.[87] using the UHF approximation combined with the 6-31G(d,p) and 6-31+G(d,p) basis sets.

First, it can be observed that the calculated geometric parameters do not vary a lot as a function of the level of theory. For example, the O_1O_2 bond lengths estimated at the B3LYP/6-31G(d,p) and MP2/6-311+G(d,p) levels of theory are 1.321 and 1.295 Å, respectively. All the optimized geometric parameters are consistent to the ones reported by Garcia et al.[87] and Murakami et al.[61] The O_1O_2 and O_2C_1 key bond lengths in B3LYP geometries are slightly longer than those in MP2 and MPW1K geometries. A similar but not such a marked trend is observed for the C_1C_2 and C_1H_1 bond lengths.

Transition State. The TS for isomerization of benzylperoxy to benzyl hydroperoxide radical is a four-member ring. The unpaired electron on the OO σ-bond attacks one of the CH σ-bonds of the methyl fragment. The two electrons in the CH bond become unpaired, and one of these pairs with the peroxy function electron to form the OH bond in the benzyl hydroperoxide radical. The peroxy function approach is calculated to occur nearly in the plane containing the $C_1H_1O_1O_2$ atoms. Structural parameters depend slightly on the level of theory. The O_1O_2 bond length in the transition state is shorter than the O_1O_2 bond length in the benzyl hydroperoxide radical, but the H_1O_1 bond in TS is longer than the H_1O_1 bond in the benzyl hydroperoxide radical. Application of diffuse functions tends to make a transition structure more reactant-like. In addition, the MP2 method predicts a transition state on the potential energy surface more reactant-like than that predicted by the B3LYP and MPW1K methods. Our optimized structures using the B3LYP levels are similar to the one reported at the B3LYP/6-311G(2d,d,p) level by Murakami et al.[61]

Benzyl Hydroperoxide Radical. The global minimum is found with the MP2 and MPW1K methods in a conformation allowing the intramolecular interaction between the oxygen and hydrogen atoms (i.e. O_2H_3 and H_2O_1). Geometry optimizations at the B3LYP levels predict the absence of this stationary point on the potential energy surface. The same results have been observed by Murakami et al.[61] Instead of the energy minimization, the O_2O_1 bond cleaves to form the molecular complex $C_6H_5CH(O)\cdots OH$ although IRC calculations from the TS structure indicate that the B3LYP transition state does not connect the isomerization transition state with the $C_6H_5CH(O)\cdots OH$ molecular complex. Despite exhaustive searches involving relaxed scans and IRC calculations, we were not able to locate a $C_6H_5\dot{C}HO_2H$ structure using the B3LYP method. Theoretical studies on the four-center isomerization of some alkylperoxy radicals did not report any optimized structure for the $R\dot{C}HO_2H$ radical when using

TABLE 1: Selected Bond Lengths in Degrees for the Benzylperoxy Radical (Reactant R), the Transition State (TS), and the Benzyl Hydroperoxide Radical (Product P)

		coordinate														
		O_1O_2			O_2C_1			C_1C_2			H_1O_1			C_1H_1		
basis set	method	R	*TS*	P	R	*TS*	P	R	*TS*	P	R	*TS*	P	R	*TS*	P
6-31G(d,p)	B3LYP	1.321	*1.493*	×	1.478	*1.392*	×	1.500	*1.469*	×	2.529	*1.332*	×	1.093	*1.299*	×
	MPW1K	1.293	*1.447*	1.412	1.443	*1.375*	1.351	1.491	*1.462*	1.402	2.513	*1.298*	0.960	1.087	*1.295*	2.646
	MP2	1.312	*1.438*	1.461	1.472	*1.397*	1.371	1.493	*1.486*	1.407	2.512	*1.288*	0.972	1.089	*1.271*	2.667
6-31+G(d,p)	B3LYP	1.321	*1.494*	×	1.481	*1.394*	×	1.499	*1.469*	×	2.529	*1.342*	×	1.093	*1.298*	×
	MPW1K	1.292	*1.445*	1.410	1.445	*1.376*	1.352	1.491	*1.462*	1.403	2.505	*1.305*	0.960	1.087	*1.295*	2.693
	MP2	1.312	*1.437*	1.466	1.479	*1.399*	1.372	1.492	*1.489*	1.410	2.523	*1.295*	0.973	1.089	*1.271*	2.742
6-31++G(d,p)	B3LYP	1.321	*1.494*	×	1.481	*1.394*	×	1.499	*1.469*	×	2.529	*1.342*	×	1.093	*1.298*	×
	MPW1K	1.292	*1.445*	1.410	1.445	*1.376*	1.352	1.491	*1.462*	1.403	2.501	*1.305*	0.960	1.087	*1.295*	2.695
	MP2	1.312	*1.437*	1.466	1.479	*1.399*	1.372	1.493	*1.489*	1.410	2.523	*1.296*	0.973	1.089	*1.271*	2.738
6-311G(d,p)	B3LYP	1.315	*1.491*	×	1.478	*1.388*	×	1.497	*1.467*	×	2.521	*1.336*	×	1.091	*1.298*	×
	MPW1K	1.285	*1.440*	1.403	1.445	*1.371*	1.349	1.489	*1.460*	1.399	2.507	*1.300*	0.957	1.086	*1.297*	2.671
	MP2	1.295	*1.429*	1.445	1.465	*1.386*	1.361	1.496	*1.491*	1.409	2.509	*1.287*	0.966	1.092	*1.274*	2.657
6-311+G(d,p)	B3LYP	1.315	*1.490*	×	1.481	*1.389*	×	1.497	*1.466*	×	2.531	*1.343*	×	1.091	*1.301*	×
	MPW1K	1.285	*1.439*	1.403	1.444	*1.371*	1.350	1.489	*1.460*	1.399	2.507	*1.306*	0.957	1.086	*1.297*	2.732
	MP2	1.295	*1.428*	1.450	1.470	*1.388*	1.362	1.500	*1.491*	1.411	2.518	*1.294*	0.968	1.092	*1.274*	2.763
cc-pVDZ	B3LYP	1.315	*1.490*	×	1.476	*1.390*	×	1.500	*1.470*	×	2.541	*1.336*	×	1.099	*1.304*	×
	MPW1K	1.287	*1.445*	1.405	1.439	*1.373*	1.351	1.491	*1.462*	1.403	2.550	*1.300*	0.964	1.093	*1.299*	2.674
	MP2	1.301	*1.434*	1.454	1.466	*1.392*	1.366	1.500	*1.494*	1.414	2.488	*1.292*	0.974	1.101	*1.277*	2.666

TABLE 2: Reaction Enthalpies $\Delta_r H$ Calculated at 0 K in kJ mol^{-1} at Different Levels of Theory

	basis set					
level of theory	6-31G(d,p)	6-31+G(d,p)	6-31++G(d,p)	6-311G(d,p)	6-311+G(d,p)	cc-pVDZ
MPW1K/"basis Set"	11.1	8.7	8.6	8.4	8.0	10.5
PMP2/"basis Set"	10.9	10.2	9.8	10.7	10.1	11.1

TABLE 3: Vibrationally Adiabatic Barriers E_0 Calculated in kJ mol^{-1} at Different Levels of Theory

	basis set					
level of theory	6-31G(d,p)	6-31+G(d,p)	6-31++G(d,p)	6-311G(d,p)	6-311+G(d,p)	cc-pVDZ
B3LYP/"basis set"	159.7	160.1	159.9	162.1	162.3	155.6
CCSD(T)/6-31G(d,p)//B3LYP/"basis set"	178.7	178.6	178.6	177.7	177.9	178.7
CASPT2/ANO-L-VDZP//B3LYP/"basis set"	145.0	145.1	145.2	143.3	141.6	137.1
MPW1K/"basis set"	174.1	174.7	174.4	175.6	176.2	170.0
CCSD(T)/6-31G(d,p)//MPW1K/"basis set"	178.4	178.9	179.0	178.0	178.6	177.7
CASPT2/ANO-L-VDZP//MPW1K/"basis set"	143.1	139.3	139.2	139.7	139.5	138.4
PMP2/"basis set"	196.9	201.0	200.2	201.0	204.2	194.5
CCSD(T)/6-31G(d,p)//PMP2/"basis set"	218.6	216.9	217.0	217.4	216.5	211.2
CASPT2/ANO-L-VDZP//PMP2/"basis set"	182.9	180.5	180.7	180.2	179.8	172.3

TABLE 4: Calculated Rate Constants at 773 K in Seconds at Different Levels of Theory

	basis set					
level of theory	6-31G(d,p)	6-31+G(d,p)	6-31++G(d,p)	6-311G(d,p)	6-311+G(d,p)	cc-pVDZ
B3LYP/"basis set"	7.51×10^{1}	1.04×10^{2}	1.07×10^{2}	5.97×10^{1}	7.19×10^{1}	1.40×10^{2}
CCSD(T)/6-31G(d,p)//B3LYP/"basis set"	3.90×10^{0}	5.92×10^{0}	5.77×10^{0}	5.26×10^{0}	6.36×10^{0}	3.85×10^{0}
CASPT2/ANO-L-VDZP//B3LYP/"basis set"	7.34×10^{2}	1.08×10^{3}	1.05×10^{3}	1.11×10^{3}	1.79×10^{3}	2.51×10^{3}
MPW1K/"basis set"	5.37×10^{0}	8.64×10^{0}	8.88×10^{0}	6.65×10^{0}	6.98×10^{0}	6.83×10^{0}
CCSD(T)/6-31G(d,p)//MPW1K/"basis set"	2.74×10^{0}	4.46×10^{0}	4.36×10^{0}	4.52×10^{0}	4.77×10^{0}	2.06×10^{0}
CASPT2/ANO-L-VDZP//MPW1K/"basis set"	6.68×10^{2}	2.13×10^{3}	2.13×10^{3}	1.77×10^{3}	2.09×10^{3}	9.27×10^{2}
PMP2/"basis set"	7.27×10^{-2}	8.13×10^{-2}	8.09×10^{-2}	4.88×10^{-2}	4.55×10^{-2}	2.93×10^{-2}
CCSD(T)/6-31G(d,p)//MP2/"basis set"	2.48×10^{-3}	6.80×10^{-3}	5.93×10^{-3}	3.76×10^{-3}	6.76×10^{-3}	2.15×10^{-3}
CASPT2/ANO-L-VDZP//PMP2/"basis set"	6.46×10^{-1}	1.96×10^{0}	1.69×10^{0}	1.24×10^{0}	2.04×10^{0}	6.17×10^{-1}
Ellis et al.[54]	2.8×10^{3}					

the B3LYP method.[56–59] From these results, the B3LYP method seems not to be adequate to obtain optimized $R\dot{C}HO_2H$ structures.

Bond lengths in MP2 geometries are longer than those in MPW1K geometries except CC bonds in the aromatic ring. The H_1O_1, O_2C_1, and O_1O_2 bonds in MP2 geometries are longer than those in MPW1K geometries by 0.009−0.013, 0.012−0.020, and 0.042−0.056 Å, respectively. The C_1C_2 bond in the benzyl hydroperoxide radical is ca. 1.406 Å, which is far shorter than the MP2/6-31G(d,p) calculated C−C bond in the benzaldehyde (value ca. 1.478 Å[88]) and the experimental C−C bond in the toluene (value ca. 1.513 Å[89]). By comparison to the C═C value in the toluene (ca. 1.395 Å[89]), our C_1C_2 bond acts indeed as a double C═C bond because of the delocalized electron. Differences of bond angles and dihedral angles are within 5° between MP2 and MPW1K geometries.

Vibrational Frequencies. Unscaled vibrational frequencies for these species are presented in Tables 9S−16S of the Supporting Information. The eigenvector in the TS corresponding to the imaginary frequency is primarily a motion of the reactive hydrogen atom being transferred from the C_1 to the O_1 centers. Whatever the method, the calculated imaginary frequency does not depend on the basis set size. The values calculated at the MP2 levels are about 25 and 15% larger than those obtained at the B3LYP and MPW1K levels, respectively. Vibrational frequencies have been scaled using appropriate scaling factors[88] for the computation of the partition functions as a function of the temperature. Their values are given in Table 17S of the Supporting Information.

III.2. Energetics. Table 2 lists the reaction enthalpies ($\Delta_r H$) computed at 0 K. The results obtained with the MPW1K method indicate that adding diffuse functions to the basis sets or increasing the basis set size has a small effect on the calculated reaction enthalpy ($\Delta\Delta_r H \leq 3.1$ kJ mol^{-1}). This trend is less important when using the MP2 method ($\Delta\Delta_r H < 1.3$ kJ mol^{-1}). We noticed that the reaction is predicted to be endothermic whatever the level of theory. Our computed reaction enthalpy at 0 K is 10.1 kJ mol^{-1} at the MP2/6-311+G(d,p) level, which is lower than the value calculated by Clothier et al.[60] at the ROMP2/3-21G//ROHF/3-21G level (i.e., 33 kJ mol^{-1}).

Table 3 shows the computed vibrationally adiabatic barriers, E_0, for the reaction under study. The following relation defines these barriers:

$$E_0 = E_{TS} - E_R + ZPE_{TS} - ZPE_R \qquad \text{(III-1)}$$

where E_{TS} and E_R are the computed energies of the TS and reactant, whereas $ZPE_{TS}$and ZPE_R are their corresponding zero-point energy corrections.

The four-center isomerization appears to have a large electronic barrier. The calculated values with one method and six different basis sets are very consistent. If we compare the results obtained using the double ζ basis sets, 6-31G(d,p) and cc-pVDZ, it can be seen that the barriers decrease slightly. The E_0's calculated with the B3LYP density functional are systematically lower by about 14−40 kJ mol^{-1} when compared to those obtained with the MPW1K density functional and the correlated ab initio method PMP2. The barriers calculated at the CCSD(T)//B3LYP levels are very close to the ones computed at the CCSD(T)//MPW1K levels but are lower by about 38 kJ mol^{-1} than those obtained at the CCSD(T)//PMP2 levels. Similar results are observed with the CASPT2 method although the barriers are lower compared to those calculated with the CCSD(T) method. We found also the UMP2 method was unsuitable because of severe spin contamination for the TS, with an expectation value of S^2 between 1.21 and 1.25, instead of

$<S^2> = S(S + 1) = 0.75$, whereas after spin projection, the $<S^2>$ values are 1.10. The barriers calculated by Clothier et al.[60] at the ROMP2/3-21G//ROHF/3-21G level and Murakami et al.[61] at the CBS-QB3 level were 121 and 161.9 kJ mol^{-1}, respectively. By comparison to our values, none of our levels of theory converge toward the value reported by Clothier et al.[60] The vibrationally adiabatic barriers computed at the B3LYP levels are very close to the one reported by Murakami et al.[61] at the CBS-QB3 level. All the values calculated here apparently seem to diverge, but it can be observed that for one given method there is little influence of the basis set size. For an accurate rate constant estimation, it is essential to choose the appropriate level of theory. In the literature, only one determination at 773 K of the rate constant for the benzylperoxy isomerization reaction is available.[54] Thus, the calculations of the rate constants with different methods are essential to allow us an assessment of the appropriate level of theory (see section III.3). It is worth noticing that the CASPT2-computed energy barriers from intramolecular abstraction are lower than those in alkylperoxy radical systems because of the weak benzyl−H bond energy resulting from resonance.

III.3. Kinetic Parameters Calculations. ***Rate Constants.*** Table 4 lists the calculated high-pressure limit rate constants at 773 K for each level of theory together with the literature value. As presented in Table 4, the computed rate constants range from 10^{-3} to 10^{3} s^{-1}, showing the strong dependence of the rate constant on the level of theory. As discussed before, the MP2 method is unsuitable because of severe spin contamination in the TS. The calculated rate constants using CCSD(T) energies on the density functional geometries are, at 773 K, 3 orders of magnitude lower than the experimental value. We observe at 773 K a very good agreement between the experimental value of 2.8×10^{3} s^{-1} (obtained at $P = 0.67$ bar) and our high-pressure limit calculated values at the CASPT2//B3LYP and CASPT2//MPW1K levels which range from 6.68×10^{2} to 2.51×10^{3} s^{-1}. By comparison to the experimental value, the most appropriate level of theory is the CASPT2/ANO-L-VDZP//B3LYP/cc-pVDZ. Murakami et al.[61] calculated the high-pressure limit rate constants at six different temperatures (300, 500, 700, 1000, 1200, and 1500 K). Using these values, one can derive from a linear regression the value at 773 K ($k = 1.23 \times 10^{1}$ s^{-1}), which is 200 times lower than the value calculated using the CASPT2 method. To conclude, we recommend the use of the CASPT2/ANO-L-VDZP//B3LYP/cc-pVDZ level of theory to compute quantitatively the temperature dependence of the high-pressure limit rate constant of the four-center isomerization of the benzylperoxy radical. Table 5 lists the calculated rate constants over the temperature range 600−2000 K.

Arrhenius Parameters. The rate constants calculated at the CASPT2/ANO-L-VDZP//B3LYP/cc-pVDZ level of theory were fitted to a three-parameter Arrhenius expression by the least squares, giving the following relation (in units of s^{-1}):

$$k(600 - 2000\ \mathrm{K}) = (1.29 \times 10^{10}) T^{0.79} \exp[-133.1\ \text{in kJ mol}^{-1})/RT] \quad \text{(III-2)}$$

Given the excellent agreement with the experimental rate constant at 773 K (see section), we recommend the Arrhenius parameters computed here for use in the thermokinetic models involving aromatic compounds. In addition, this excellent agreement gives us confidence in our predicted kinetic parameters.

IV. Conclusions

Ab initio and DFT theoretical calculations combined with canonical TST were performed on the reaction of the four-center isomerization of the benzylperoxy radical. The geometry parameters for the reactant, the product, and the TS were fully optimized with the B3LYP, MPW1K, and MP2 methods combined with six different basis sets. The calculation of the energetics of the reaction proved to be more dependent on the level of theory than on the nature and extent of the basis set. The use of the MP2 method is unsuitable because of severe spin contamination in the TS. The high-pressure limit calculated rate constant at 773 K with a Wigner tunneling correction using CASPT2 on density functional geometries is in very good agreement with the experimental value. In addition, we recommend using the CASPT2/ANO-L-VDZP//B3LYP/cc-pVDZ level of theory to calculate the kinetic parameters as a function of the temperature. In this article, we showed that standard theoretical methods were not adequate to obtain quantitative rate constants for the reaction under study. The use of the elaborated CASPT2 method was crucial to estimate a quantitative rate constant.

TABLE 5: Calculated Rate Constants over the Temperature Range 600−2000 K at the CASPT2/ANO-L-VDZP//B3LYP/cc-pVDZ Level of Theory

T (K)	k (s^{-1})
600	5.31×10^{0}
700	2.69×10^{2}
800	5.19×10^{3}
900	4.26×10^{4}
1000	3.39×10^{5}
1100	1.57×10^{6}
1200	5.67×10^{6}
1300	1.69×10^{7}
1400	4.32×10^{7}
1500	9.77×10^{7}
1600	2.00×10^{8}
1700	3.78×10^{8}
1800	6.65×10^{8}
1900	1.10×10^{9}
2000	1.74×10^{9}

Acknowledgment. We thank the Institut du Développement et des Ressources en Informatique Scientifique, the Centre de Ressources Informatiques de Haute Normandie, and the Centre de Ressources Informatiques of the University of Lille 1 for providing computing time for part of the theoretical calculations. We thank the Nord Pas de Calais Region, the European funds for Regional Economic Development, and the Air Quality Program of Institut de Recherche en Environnment Industriel for their financial support. We thank Dr. Thibaud Cours (University of Reims) for fruitful discussions. We also thank the anonymous reviewers for their useful comments.

Supporting Information Available: Optimized geometry parameters, and vibrational frequencies are given for the benzylperoxy radical, the benzyl hydroperoxide radical, and the transition state. The vibrational scaling factors are also listed. This material is available free of charge via the Internet at http://pubs.acs.org.

References and Notes

(1) Guibet, J.-C. *Carburants et Moteurs: Technologies, Energie, Environnement*; Editions Technip: Paris, 1997; pp 51−61.

(2) Off. J. Eur. Union. http://eur-lex.europa.eu/LexUriServ/site/fr/oj/2003/l_076/l_07620030322fr00100019.pdf. (Accessed Nov 2007).

(3) Prado, G.; Garo, A.; Ko, A.; Sarofim, A. *Symp. (Int.) Combust., [Proc.]* **1985**, *20*, 989–996.

(4) Bockhorn, H.; Fetting, F.; Wenz, H. W. *Ber. Bunsen-Ges. Phys. Chem.* **1983**, *87*, 1067–1073.
(5) Bittner, J. D.; Howard, J. B. *Symp. (Int.) Combust., [Proc.]* **1981**, *18*, 1105–1116.
(6) Ciajolo, A.; D'Anna, A.; Barella, R. *Combust. Sci. Technol.* **1994**, *100*, 271–281.
(7) Ciajolo, A.; Barbella, R.; Tregrossi, A.; Bonfanti, L. *Symp. (Int.) Combust., [Proc.]* **1998**, *27*, 1481–1487.
(8) Biordi, J. C.; Lazzara, C. P.; Papp, J. F. *Symp. (Int.) Combust., [Proc.]* **1977**, *16*, 1097–1109.
(9) D'Alessio, A.; Di Lorenzo, A.; Sarofim, A. F.; Beretta, F.; Masi, S.; Venitozzi, C. *Symp. (Int.) Combust., [Proc.]* **1974**, *15*, 1427–1438.
(10) D'Anna, A.; D'Alessio, A.; Minatolo, P. In *Soot Formation in Combustion: Mechanisms and Models*; Bockhorn, H., Ed., Springer-Verlag: Heidelberg, Germany, 1994; pp 83−103.
(11) Senkan, S. M.; Castaldi, M. J. *Combust. Flame* **1996**, *107*, 141–150.
(12) Marinov, N. M.; Pitz, W. J.; Westbrook, C. K.; Castaldi, M. J.; Senkan, S. M. *Combust. Sci. Technol.* **1996**, *116*−*117*, 211–287.
(13) Melton, T. R.; Vincitore, A. M.; Senkan, S. M. *Symp. (Int.) Combust., [Proc.]* **1998**, *27*, 1631–1637.
(14) Xu, F.; Lin, K.-C.; Faeth, G. M. *Combust. Flame* **1998**, *115*, 195–209.
(15) Frenklach, M. *Phys. Chem. Chem. Phys.* **2002**, *4*, 2028–2037.
(16) Fahmy, O. G.; Fahmy, M. J. *Cancer Res.* **1973**, *33*, 302–309.
(17) Denissenko, M. F.; Pao, Tang, M.-A.; Pfeifer, G. P. *Science* **1996**, *274*, 430–432.
(18) Durant, J. L.; Busby, W. F.; Lafleur, A. L.; Penman, B. W.; Crespi, C. L. *Mutat. Res.* **1996**, *371*, 123–157.
(19) El Bakali, A.; Dupont, L.; Lefort, B.; Lamoureux, N.; Pauwels, J.-F.; Montero, M. *J. Phys. Chem. A* **2007**, *111*, 3907–3921.
(20) El Bakali, A.; Ribaucour, M.; Saylam, A.; Vanhove, G.; Therssen, E.; Pauwels, J.-F. *Fuel* **2006**, *85*, 881–895.
(21) Morley, C.; Pilling, M. J. Introduction. In *Low-Temperature Combustion and Autoignition*; Compton, R. G., Hancock, G., Eds.; Comprehensive Chemical Kinetics Series; Elsevier Science: Amsterdam, 1997; Vol. 35, pp XI−XVI.
(22) Westbrook, C. K. *Symp. (Int.) Combust., [Proc.]* **2000**, *28*, 1563–1577.
(23) El Bakali, A.; Dagaut, P.; Pillier, L.; Desgroux, P.; Pauwels, J.-F. *Combust. Flame* **2004**, *137*, 109–128.
(24) El Bakali, A.; Pillier, L.; Desgroux, P.; Gasnot, L.; Pauwels, J.-F.; Da Costa, I. *Fuel* **2006**, *85*, 896–909.
(25) Dagaut, P; El Bakali, A.; Ristori, A. *Fuel* **2006**, *85*, 944–956.
(26) Dupont, L.; El Bakali, A.; Pauwels, J.-F.; Da Costa, I.; Meunier, P.; Richter, H. *Combust. Flame* **2003**, *135*, 171–183.
(27) Minetti, R.; Ribaucour, M.; Carlier, M.; Fittschen, C.; Sochet, L.-R. *Combust. Flame* **1994**, *96*, 201–211.
(28) Ribaucour, M.; Minetti, R.; Sochet, L.-R. *Symp. (Int.) Combust., [Proc.]* **1998**, *27*, 345–351.
(29) Ribaucour, M.; Roubaud, A.; Minetti, R. *Symp. (Int.) Combust., [Proc.]* **2000**, *28*, 1701–1707.
(30) Ribaucour, M.; Lemaire, O.; Minetti, R. *Symp. (Int.) Combust., [Proc.]* **2002**, *29*, 1303–1310.
(31) Barnard, J. A.; Ibberson, V. A. *Combust. Flame* **1965**, *9*, 149–157.
(32) Ciajolo, A.; D'Anna, A.; Mercogliano, R. *Combust. Sci. Technol.* **1993**, *90*, 357–371.
(33) Roubaud, A.; Lemaire, O.; Minetti, R.; Sochet, L.-R. *Combust. Flame* **2000**, *123*, 561–571.
(34) Brezinsky, K. *Prog. Energy Combust. Sci.* **1986**, *12*, 1–24.
(35) Emdee, J. L.; Brezinsky, K.; Glassman, I. *J. Phys. Chem.* **1992**, *96*, 2151–2161.
(36) McLain, A. G.; Jachimowski, C. F.; Wilson, C. H. Chemical Kinetic Modeling of Benzene and Toluene Oxidation behind Shock Waves; NASA Technical Paper 1472; National Aeronautics and Space Administration: Washington, D.C., 1979.
(37) Asaba, T.; Fujii, N. *Symp. (Int.) Combust., [Proc.]* **1971**, *13*, 155–164.
(38) Fujii, N.; Asaba, T. *Symp. (Int.) Combust., [Proc.]* **1973**, *14*, 433–442.
(39) Bittker, D. A. Detailed Mechanism of Benzene Oxidation; NASA Technical Paper 100202; National Aeronautics and Space Administration: Washington, D.C., 1987.
(40) Bittker, D. A. *Combust. Sci. Technol.* **1991**, *79*, 49–72.
(41) Bittker, D. A. Oxidation Mechanisms of Toluene and Benzene; NASA Technical Paper 3546; National Aeronautics and Space Administration: Washington, D.C., 1995.
(42) Klotz, S. D.; Brezinsky, K.; Glassman, I. *Symp. (Int.) Combust., [Proc.]* **1998**, *27*, 337–344.
(43) Pitz, W. J.; Seiser, R.; Bozzelli, J. W.; Da Costa, I.; Fournet, R.; Billaud, F.; Battin-Leclerc, F.; Seshadri, K.; Westbrook, K. The Second Joint Meeting of the US Sections of the Combustion Institute, Oakland, CA, March 25−28, 2001.
(44) Sivaramakrishnan, R.; Tranter, R. S.; Brezinsky, I. *Proc. Combust. Inst.* **2005**, *30*, 1165–1173.
(45) Lindstedt, R. P.; Maurice, L. Q. *Combust. Sci. Technol.* **1996**, *120*, 119–167.
(46) Shandross, R.; Longwell, J. P.; Howard, J. B. *Symp. (Int.) Combust., [Proc.]* **1996**, *26*, 711–719.
(47) Lindstedt, R. P.; Skevis, G. *Combust. Flame* **1994**, *99*, 551–561.
(48) Ristori, A.; Dagaut, P.; Pengloan, G.; El Bakali, A.; Cathonnet, M. *Combustion* **2001**, *1*, 265–294.
(49) Dagaut, P.; Ristori, A.; El Bakali, A.; Cathonnet, M. *Fuel* **2002**, *81*, 173–184.
(50) Gaïl, S.; Dagaut, P. *Combust. Flame* **2005**, *141*, 281–297.
(51) Battin-Leclerc, F.; Bounaceur, R.; Belmekki, N.; Glaude, P. A. *Int. J. Chem. Kinet.* **2006**, *38*, 284–302.
(52) Benson, S. W. *Prog. Energy Combust. Sci.* **1981**, *7*, 125–134.
(53) Roubaud, A. Etude de l'oxydation et la combustion de quelques hydrocarbures aromatiques entrant dans la composition des carburants automobiles. Ph.D. Thesis, Université des Sciences et Technologies de Lille, Villeneuve d'Ascq, France, January 29, 1999.
(54) Ellis, C. M.; Scott, S.; Walker, R. W. *Combust. Flame* **2003**, *132*, 291–304.
(55) Chan, W.-T.; Hamilton, I. P.; Pritchard, H. O. *J. Chem. Soc., Faraday Trans.* **1998**, *94*, 2303–2306.
(56) Sheng, C. Y.; Bozzelli, J. W.; Dean, A. M.; Chang, A. Y. *J. Phys. Chem. A* **2002**, *106*, 7276–7293.
(57) Sun, H.; Bozzelli, J. W. *J. Phys. Chem. A* **2004**, *108*, 1694–1711.
(58) Lee, J.; Bozzelli, J. W. *Proc. Combust. Inst.* **2005**, *30*, 1015–1022.
(59) Zhu, L.; Bozzelli, J. W.; Kardos, L. M. *J. Phys. Chem. A* **2007**, *111*, 6361–6377.
(60) Clothier, P. Q. E.; Shen, D.; Pritchard, H. O. *Combust. Flame* **1995**, *101*, 383–386.
(61) Murakami, Y.; Oguchi, T.; Hashimoto, K; Nosaka, Y. *J. Phys. Chem. A* **2007**, *111*, 13200–13208.
(62) Frisch, M. J.; Trucks, G. W.; Schlegel, H. B.; Scuseria, G. E.; Robb, M. A.; Cheeseman, J. R.; Montgomery, J. A., Jr.; Vreven, T.; Kudin, K. N.; Burant, J. C.; Millam, J. M.; Iyengar, S. S.; Tomasi, J.; Barone, V.; Mennucci, B.; Cossi, M.; Scalmani, G.; Rega, N.; Petersson, G. A.; Nakatsuji, H.; Hada, M.; Ehara, M.; Toyota, K.; Fukuda, R.; Hasegawa, J.; Ishida, M.; Nakajima, T.; Honda, Y.; Kitao, O.; Nakai, H.; Klene, M.; Li, X.; Knox, J. E.; Hratchian, H. P.; Cross, J. B.; Bakken, V.; Adamo, C.; Jaramillo, J.; Gomperts, R.; Stratmann, R. E.; Yazyev, O.; Austin, A. J.; Cammi, R.; Pomelli, C.; Ochterski, J. W.; Ayala, P. Y.; Morokuma, K.; Voth, G. A.; Salvador, P.; Dannenberg, J. J.; Zakrzewski, V. G.; Dapprich, S.; Daniels, A. D.; Strain, M. C.; Farkas, O.; Malick, D. K.; Rabuck, A. D.; Raghavachari, K.; Foresman, J. B.; Ortiz, J. V.; Cui, Q.; Baboul, A. G.; Clifford, S.; Cioslowski, J.; Stefanov, B. B.; Liu, G.; Liashenko, A.; Piskorz, P.; Komaromi, I.; Martin, R. L.; Fox, D. J.; Keith, T.; Al-Laham, M. A.; Peng, C. Y.; Nanayakkara, A.; Challacombe, M.; Gill, P. M. W.; Johnson, B.; Chen, W.; Wong, M. W.; Gonzalez, C.; Pople, J. A. Gaussian 03, revision D.01; Gaussian, Inc.: Wallingford, CT, 2004.
(63) Karlström, G.; Lindh, R.; Malmqvist, P.-A.; Roos, B. O.; Ryde, U.; Veryazov, V.; Widmark, P.-O.; Cossi, M.; Schimmelpfennig, B.; Neogrady, P.; Seijo, L. *Comput. Mater. Sci.* **2003**, *28*, 222–239.
(64) Lee, C.; Yang, W.; Parr, R. *Phys. Rev. B* **1988**, *37*, 785–789.
(65) Becke, A. *J. Chem. Phys.* **1993**, *98*, 5648–5652.
(66) Lynch, B. J.; Fast, P. L.; Harris, M.; Truhlar, D. G. *J. Phys. Chem. A* **2000**, *104*, 4811–4815.
(67) Møller, C.; Plesset, M. S. *Phys. Rev.* **1934**, *46*, 618–622.
(68) Descriptions of the Pople-style basis sets can be found in: Foresman, J. B.; Frisch, A. E. *Exploring Chemistry with Electronic Structure Methods*, 2nd ed.; Gaussian, Inc.: Pittsburgh, PA, 1996.
(69) (a) Dunning, T. H., Jr *J. Chem. Phys.* **1989**, *90*, 1007–1023. (b) Woon, D. E.; Dunning, T. H., Jr *J. Chem. Phys.* **1993**, *98*, 1358–1371. (c) Woon, D. E.; Dunning, T. H., Jr *J. Chem. Phys.* **1994**, *100*, 2975–2988. (d) Wilson, A. K.; Woon, D. E.; Peterson, K. A.; Dunning, T. H., Jr *J. Chem. Phys.* **1999**, *110*, 7667–7676.
(70) Gonzalez, C.; Schlegel, H. B. *J. Chem. Phys.* **1989**, *90*, 2154–2161.
(71) (a) Schlegel, H. B. *J. Chem. Phys.* **1986**, *84*, 4530–4534. (b) Schlegel, H. B. *J. Phys. Chem.* **1988**, *92*, 3075–3078. (c) Sosa, C.; Schlegel, H. B. *Int. J. Quantum Chem.* **1986**, *29*, 1001–1015. (d) Sosa, C.; Schlegel, H. B. *Int. J. Quantum Chem.* **1987**, *30*, 155–156.
(72) Cizek, J. *Chem. Phys.* **1966**, *45*, 4256–4266.
(73) Cizek, J. *Adv. Chem. Phys.* **1969**, *14*, 35–89.
(74) Purvis, G. D., III; Bartlett, R. J. *J. Chem. Phys.* **1982**, *76*, 1910–1918.
(75) Raghavachari, K.; Trucks, G. W.; Pople, J. A.; Head-Gordon, M. *Chem. Phys. Lett.* **1989**, *157*, 479–483.
(76) Roos, B. O.; Andersson, K.; Fulscher, M. P.; Malmqvist, P.-A.; Serrano-Andres, L.; Pierloot, K.; Merchan, M. *Advances in Chemical Physics*; Wiley & Sons: New York, 1996; Vol. XCIII.

(77) Andersson, K. In *Encyclopedia of Computational Chemistry*; Wiley: New York, 1998; p 460.

(78) Andersson, K.; Malmqvist, P.-A.; Roos, B.; Sadlej, A. J.; Wolinski, K. *J. Phys. Chem.* **1990**, *94*, 5483–5488.

(79) Andersson, K.; Malmqvist, P. A.; Roos, B. *J. Chem. Phys.* **1992**, *96*, 1218–1226.

(80) Widmark, P.-O.; Malmqvist, P.-A.; Roos, B. O. *Theor. Chim. Acta* **1990**, *77*, 291–306.

(81) (a) Eyring, H. J. *Chem. Phys.* **1935**, *3*, 107–115. (b) Johnston, H. S. *Gas Phase Reaction Rate Theory*; The Roland Press Co.: New York, 1966. (c) Laidler, K. J. *Theories of Chemical Reaction Rates*; McGraw-Hill: New York, 1969. (d) Weston, R. E.; Schwartz, H. A. *Chemical Kinetics*; Prentice-Hall: New York, 1972. (e) Rapp, D. *Statistical Mechanics*; Holt, Reinhard, and Winston: New York, 1972. (f) Nikitin, E. E. *Theory of Elementary Atomic and Molecular Processes in Gases*; Clarendon Press: Oxford, 1974. (g) Smith, I. W. M. *Kinetics and Dynamics of Elementary Gas Reactions*; Butterworths: London, 1980. (h) Steinfeld, J. I.; Francisco, J. S.; Hase, W. L. *Chemical Kinetics and Dynamics*; Prentice-Hall: Englewood Cliffs, NJ, 1989.

(82) Wigner, E. P. *Z. Phys. Chem.* **1932**, *B19*, 203–216.

(83) (a) Bell, R. P. *The Tunnel Effect in Chemistry*; Chapman & Hall: New York, NY, 1980. (b) Louis, F.; Gonzalez, C.; Sawerysyn, J.-P. *J. Phys. Chem. A* **2004**, *108*, 10586–10593.

(84) (a) Garrett, B. C.; Truhlar, D. G. *J. Phys. Chem.* **1979**, *83*, 2921–2926. (b) Garrett, B. C.; Truhlar, D. G. *J. Chem. Phys.* **1984**, *81*, 309–317. (c) Skodje, R. T.; Garrett, B. C.; Truhlar, D. G. *J. Phys. Chem.* **1981**, *85*, 3019–3023. (d) Skodje, R. T.; Garrett, B. C.; Truhlar, D. G. *J. Chem. Phys.* **1982**, *77*, 5955–5976. (e) Garrett, B. C.; Truhlar, D. G.; Grev, R. S.; Magnuson, A. W. *J. Phys. Chem.* **1980**, *84*, 1730–1748. (f) Garrett, B. C.; Truhlar, D. G.; Grev, R. S.; Magnuson, A. W. *J. Phys. Chem.* **1983**, *87*, 4554–4554.

(85) (a) Miller, W. H.; Shi, S.-H. *J. Chem. Phys.* **1981**, *75*, 2258–2264. (b) Miller, W. H.; Smith, F. T. *Phys. Rev.* **1978**, *A17*, 939–953.

(86) *KISTHEP 1.0*; Henon, E.; Bohr, F.; Canneaux, S.; Postat, B.; Auge, F.; Bouillard, E.; Domureau, V. University of Reims Champagne-Ardenne: France, 2003.

(87) Garcia, I.; Ruiz, M. E.; Smeyers, Y. G.; Vivier Bunge, A. *J. Mol. Struct.: THEOCHEM* **1995**, *340*, 149–158.

(88) NIST Computational Chemistry Comparison and Benchmark Database; Johnson, R. D., III, Ed.; NIST Standard Reference Database, Number 101, Release 12, Aug 2005. http://srdata.nist.gov/cccbdb.

(89) Amir-Ebrahimi, V.; Choplin, A.; Demaison, J.; Roussy, G. *J. Mol. Spectrosc.* **1981**, *89*, 42–52.

JP711231C